Chemical Methodologies 6(2022) 475-493

Chemical Methodologies

Journal homepage: http://chemmethod.com

Original Research Article

Synthesis, Characterization, Thermal Analysis and Bioactivity of Some Transition Metals Complexes with New Azo Ligand

Shaima Mohammed Reda*, **Abbas Ali Salih Al-Hamdani**

Department of Chemistry, College of Science for Women, University of Baghdad, Baghdad, Iraq

ARTICLE INFO

Article history

Submitted: 2022-04-02
Revised: 2022-04-10
Accepted: 2022-04-15
Manuscript ID: CHEMM-2204-1468
Checked for Plagiarism: **Yes**
Language Editor:
Dr. Ermia Aghaie
Editor who approved publication:
Professor Dr. lotfali saghatforoush
DOI:10.22034/CHEMM.2022.335815.1468

KEYWORDS

Bioactivity
Mass spectroscopy
Azo complexes
Spectroscopic studies
Thermal analysis

ABSTRACT

4-Amino-*N*-(5-methyl-isaxazol-3-yl)-benzenesulfonamide, a new azo (LH) ligand, was synthesized by reacting the diazonium salt of Sulfamethoxazole with coupling compound 3-amino phenol. Spectroscopic techniques (UV-Vis, FTIR, 1H &13C-NMR, and LC-Mass) as well as micro elemental analyses (C.H.N.O) and TGA and SDC were used to identify the azo ligand. Complexes of (Zn(II), Cr(III), Cu(II) and VO(II)) were produced and characterized by atomic absorption, elemental microanalysis, infrared, LC-Mass, TGA, DSC and UV-Vis spectral techniques, as well as conductivity and magnetic quantifications. All the complexes had a 1:2 metal-ligand ratio, and non-electrolytes at all complexes and tetrahedral geometry suggested except Cr-complex, which demonstrated octahedral and VO-complex that demonstrated Square pyramidal. The results of the thermal decomposition indicated the presence of coordinated water molecule for only Cr-complex. The biological activity of some prepared compounds against two types of bacteria and four types of fungi was also studied, suggesting varying inhibition values.

GRAPHICAL ABSTRACT

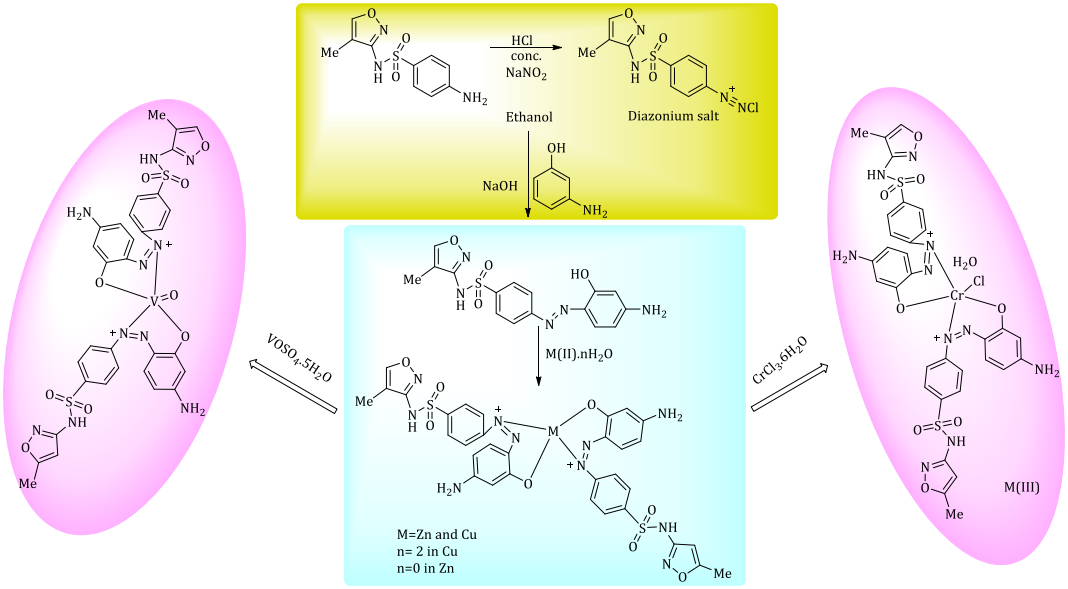

* Corresponding author: Shaima Mohammed Reda
✉ E-mail: shaimaa.mohammed1205a@csw.uobaghdad.edu.iq

Introduction

Azo entities demonstrate the wider incoming commercial dyes. It is believed that the benefit of such compounds is on the rise. Additionally, they occupy a main role that controls the azo-dyes and printing materials. These dyes result from simple means including diazotization-coupling. Various modifications were carried out in order to gain desirable-colored features [1]. Azo-dyes are widely employed dyes constituting approximately 60% of whole dyes [2,3]; 70% of all dyes applied in manufacturing are azo entities [4,5], which are distinguished by their N=N functional group [6]. Azo dyes are the most important synthetic colorants that have been widely used in textile, printing, paper manufacturing, etc. [7]. Azo entities have also been employed in textile. In addition to their harmful aspects that affect human beings, they have attracted attention for treating liquid wastes containing azo dyes in order to destroy them or convert them into useful products [8,9]. Azo compounds can be synthesized in many ways: Diazotization and coupling [10], condensation of nitro compounds with amines [2], reduction of nitro compounds [3], and oxidation of amino compounds [4]. Industrially, diazotization and azo coupling reaction are the preferred chemical routes unless the desired starting raw materials are unavailable. In the absence of the starting materials for diazotization and azo coupling, other chemical routes can be used. In this work, we have also synthesized our ligand according to diazotization and coupling method. In such reactions, strong mineral acids like H_2SO_4 and HCl in aqueous solution have been the most prevalent method to synthesize azo aromatic compounds via diazotization-azo coupling reactions [10-12]. Using mineral acids in diazotization reactions clashes with the concept of green chemistry. 3-aminophenol and sulfamethaxazol as starting materials forming (E)-3-((4-amino-2-hydroxyphenyl)diazenyl)-N-(4-methylisoxazol-3-yl)benzenesulfonamide can be classified as azo compound, which in turn coordinate with each of VO(II), Cu(II), Zn(II) and Cr(III) metal ions in 2:1 ratio.

Materials and Methods

The next chemical materials were obtainable trading products, Sulfamethoxazole, 3-aminophenol, hydrated sodium nitrate $NaNO_3$, hydrochloric acid HCl, ethanol, metal salts ($VOSO_4.5H_2O$), ($CrCl_3.6H_2O$), ($ZnCl_2$) and ($CuCl_2$), gained from F-897ewluka, sigma Aldrich. FTIR was detected in the range of 4000-400 cm^{-1} on a Shimadzu-3800 Spectro-meter. The electronic spectral data were detected by using Shimadzu160 Spectro-photometer. Mass indication analysis of compounds was carried out by LC Mass100P Shimadzu. TGA investigations of all previous forms were done on Perkin-Elmer Pyris Diamond DS/TGA. ^{1}H-NMR spectra were registered by employing Bruker 400-MHz Spectro-meter and elemental micro analysis was done on a Perkin-Elmer automatic instruments model 240B. Metals were estimated employing a Shimadzu(A-A)680G AA-spectrometer. Accessibility was measured by employing jenway4071. The chloride content was estimated gravimetrically. Magnetic features were measured using balance magnetic susceptibility model MSR-MKi.

Synthesis of azo dye ligand

The ligand in Scheme 1. was synthesized according to the suggested method by Shibata [13]. 1g, 3.948 mmol of Sulfamethoxazole was dissolved in a mixture composed of 37% (2 mL) concentrated Hydrochloric acid HCl, (15 mL) distilled water and 15 mL of ethanol. The solution was cooled from 0 °C up to 5 °C, then 10%, 1g, 14.49 mmol of hydrated Sodium Nitrite $NaNO_2$ was gradually added to the solution with continuous stirring to avoid any increase in temperature up to 5 °C, followed by leaving the solution for about 45 min. to perform the diazotization process resulting in diazonium salt; salt solution was added gradually with continuous stirring onto (0.43 g, 3.948 mmol) of 3-aminophenol dissolved in 20ml of ethanol. The change in solution into dark color was observed by keeping on stirring for about 30 min. to perform the reaction. The solution was isolated until being stable, then a few drops of sodium hydroxide was added to NaOH solution in order to equivalize the

middle of reaction till reaching 6.8pH at which the perfect precipitating of ligand occurred. Finally, the former was filtered and recrystallization was made by methanol and dried, resulting in 1.34 g, 90.70%, m.p, 192-194 °C and orange precipitate.

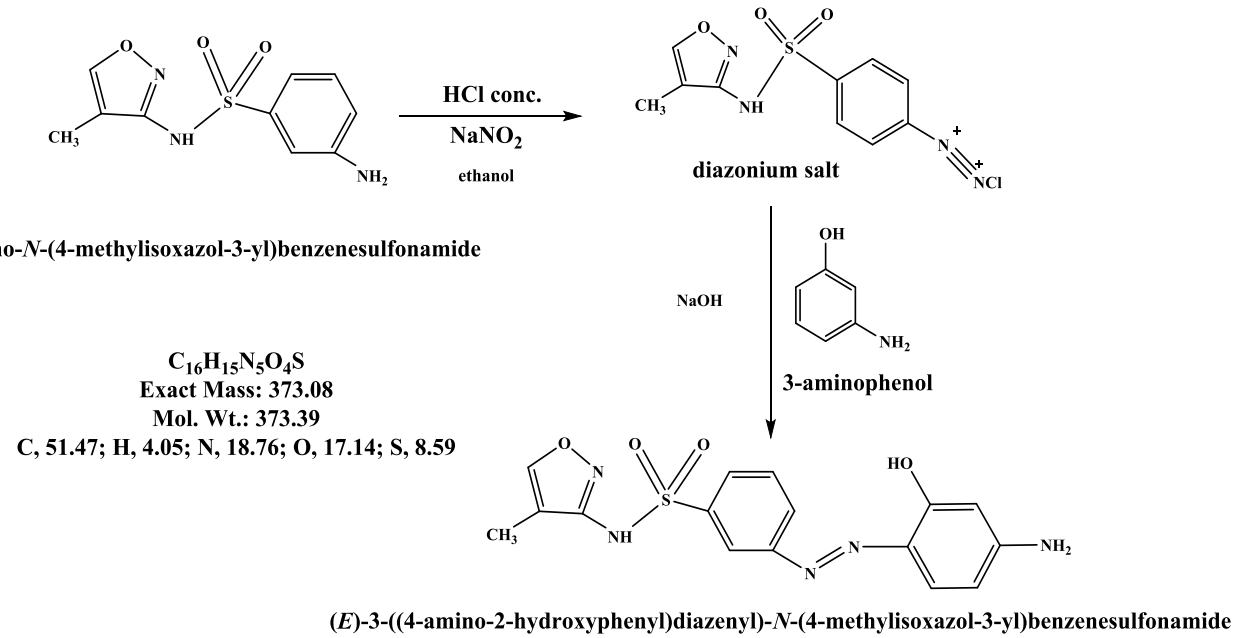

Scheme 1: Synthesis of ligand

General method for the preparation of metallic ions complexes

The metal ion complexes were made by employing their corresponded metal salts as follows: 0.00027 mol, 1 g of azo ligand dissolved in 20 mL of absolute ethanol (with continuous stirring) was gradually added dropwise to Zn(II), VO(II), Cr(II) and Cu(II) (0180 g, 0.00133 mol $ZnCl_2$ and 0.240 g $VOSO_4.5H_2O$), (0.352 g $CrCl_3.6H_2O$), (0.178 g $CuCl_2$), meant to equalize 0.00133mol. Each metal salt was used in [1:2] M:L form. The mixture was heated for 2 hours at 50-70 °C, then chilled in an ice bath until precipitated, then left overnight. To remove any unreacted components, the solid complexes were separated and washed with distilled water and a little amount of hot ethanol. Finally, vacuum desiccators were used to dry the complexes (Scheme 2). The analytical and physical properties of the ligand and its metal complexes are summarized in Table 1.

Study of Bioactivity

Some of the starting materials (ligand and employed-metal-salts) were examined for *staphylococcus aureus* (gram positive) and *Pseudomonas aeruginosa* (gram negative) bacteria and fungi such as *Penicilliumexpansum*, *Fusariumgraminearum, Macrophominaphasealina,* and *Candida albicans* through wall-agar-distribution-manner. The employed solvent was DMSO. The concentrations of the materials mentioned previously was 10^{-3} M. The tablets were evolved for 24 and 48 h pertaining to bacteria and fungi, respectively, at 37 °C.

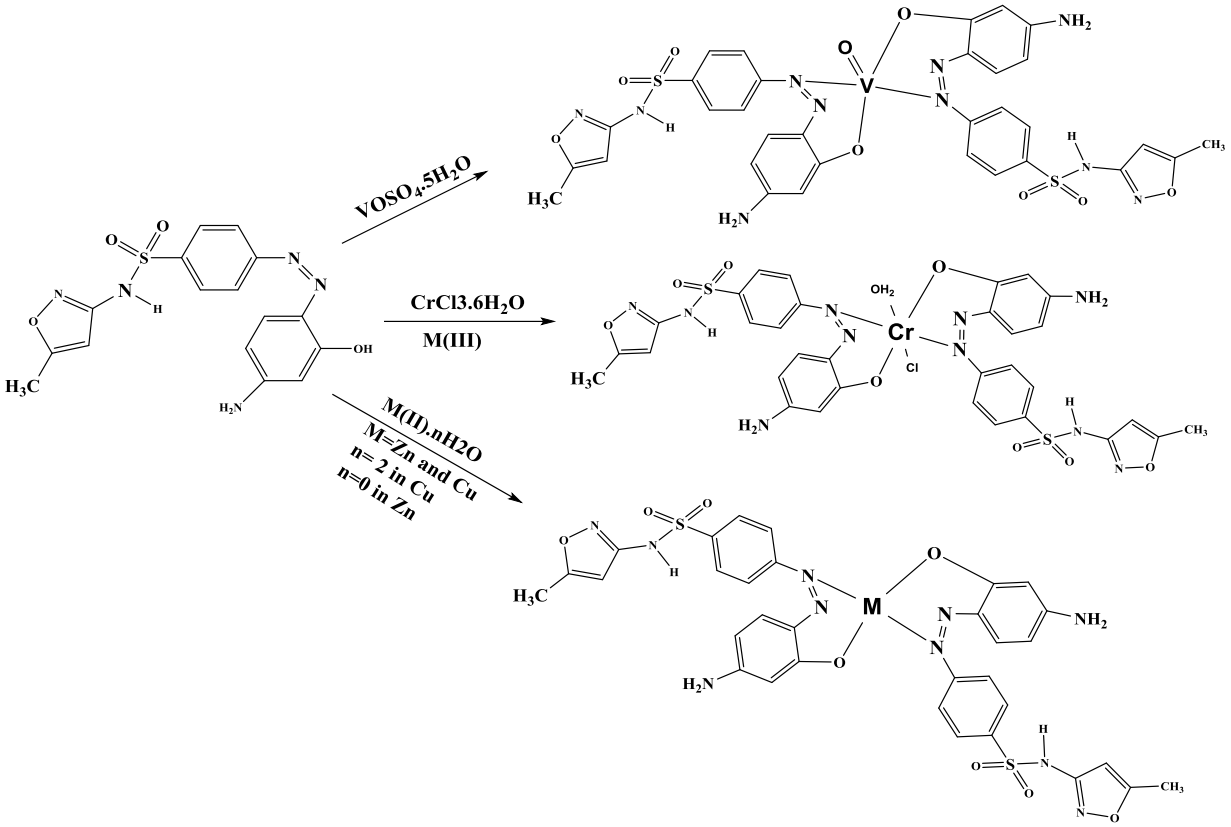

Scheme 2: Synthesis of complexes

Table 1: Physical features and analytical returns of ligand and its related complexes

Compounds formula	Micro elemental analysis (Found) and Calc.					%M	%Cl	Color	m.p (°C)	Yield (%)
	%C	%H	%N	%O	%S					
$C_{16}H_{15}N_5O_4S$	(52.44)	(4.99)	(19.01)	(16.16)	(7.40)	--	--	Orange	192-194	90.97
373.39 g/mol	51.47	4.05	18.76	17.14	8.59	--	--			
$C_{32}H_{28}N_{10}O_9S_2V$	(46.64)	(4.44)	(18.71)	(17.99)	(8.07)	(6.5)	--	Dark Brown	209d	78
811.70 g/mol	47.35	3.48	17.26	17.74	7.90	6.28	--			
$C_{32}H_{30}N_{10}CrO_9S_2Cl$	(46.04)	(4.03)	(17.01)	(16.81)	(7.79)	(6.95)	(3.88)	Olive	230-233	75
850.22 g/mol	45.20	3.56	16.47	16.94	7.45	6.12	4.17			
$C_{32}H_{28}N_{10}O_8CuS_2$	(48.19)	(2.98)	(18.78)	(16.11)	(9.07)	(8.45)	--	Reddish Brown	288d	90
808.31 g/mol	47.55	3.49	17.33	15.83	7.93	7.86	--			
$C_{32}H_{28}N_{10}O_8S_2Zn$	(46.74)	(4.41)	(16.61)	(14.64)	(8.71)	(8.88)	--	Light Brown	>325	89
810.15 g/mol	47.44	3.48	17.29	15.80	7.92	8.07	--			

d = decompose

Result and discussion

Physical and chemical properties of azo dye ligand

Azo-ligand distinguished by its non- crystalline appearance resembled high quality orange-powder, which is soluble in DMF and DMSO but it is highly soluble in ethanol. In presence of air, azo complexes and related azo bond are stable.

(^1H and ^{13}C)-NMR spectra

Figure 1 shows the ^{1}H-NMR spectra of the ligand LH in DMSO-d_6. The spectra revealed a peak at δ (2.51) ppm, which was ascribed to CH_3 chemical changes; at 5.94 ppm, the NH_2 group appears as a singlet. The proton (OH) phenolic ring was ascribed to the highest signal at (11.14) ppm. The aromatic protons of benzene groups are attributed to the numerous peaks at δ (7.78-7.80) ppm. The proton (NH) was ascribed to the highest signal at (9.51) ppm. The proton (C-H aromatic) of the besides phenol group Ar-OH is responsible for the singlet signal at δ (6.75) ppm and (C-H aromatic) of the besides phenol group Ar-NH_2 is responsible for the singlet doublet at δ (6.87) ppm. The proton (C-H aromatic) of the besides CH_3 group heterocyclic is responsible for the singlet signal at δ (5.49) ppm [14-16]. The molecular

structure is illustrated as follows: **^{13}C-**NMR (DMSO, ppm): 15.16(C-1), 174.60(C-2), 107.50(C-3), 167.70(C-4), 162.15(C-5), 131.97(C-6 C-7), 132.02(C-8), 146.94(C-9), 148.76(C-10), 157.27(C-11), 134.31(C-12), 115.39(C-13), 121.95(C-14), 151.10(C-15), 153.24(C-16).

^{1}H-MNR spectrum of zinc complex in Figure 2 demonstrates a singlet signal belonging to (N-H) group 2H at δ 8.55 ppm, multiplate signal at 8.01-7.58 ppm belonging to 8H of aromatic C-H group, singlet signal belonging to aromatic 2H of C-H group being close to phenolic group at δ 6.71 ppm, doublet signal belonging to 4H of aromatic ring C-H being close to primary amine group at δ 6.94 ppm, singlet signal belonging to 4H of primary amine (Ar-NH_2) at δ 5.52 ppm, another singlet signal belonging to 2H of C-H group present in hetero ring at δ 5.25 ppm, and singlet signal belonging to 6H of terminal CH_3 group at δ 2.61 ppm in addition to the presence of solvent signal at δ 2.51 ppm. The disappearance of phenolic group OH signal and presence of NH_2 signal is some evidence indicating the occurrence of coordination through phenolic oxygen and that the primary amine group does not coordinate with metal ion [14].

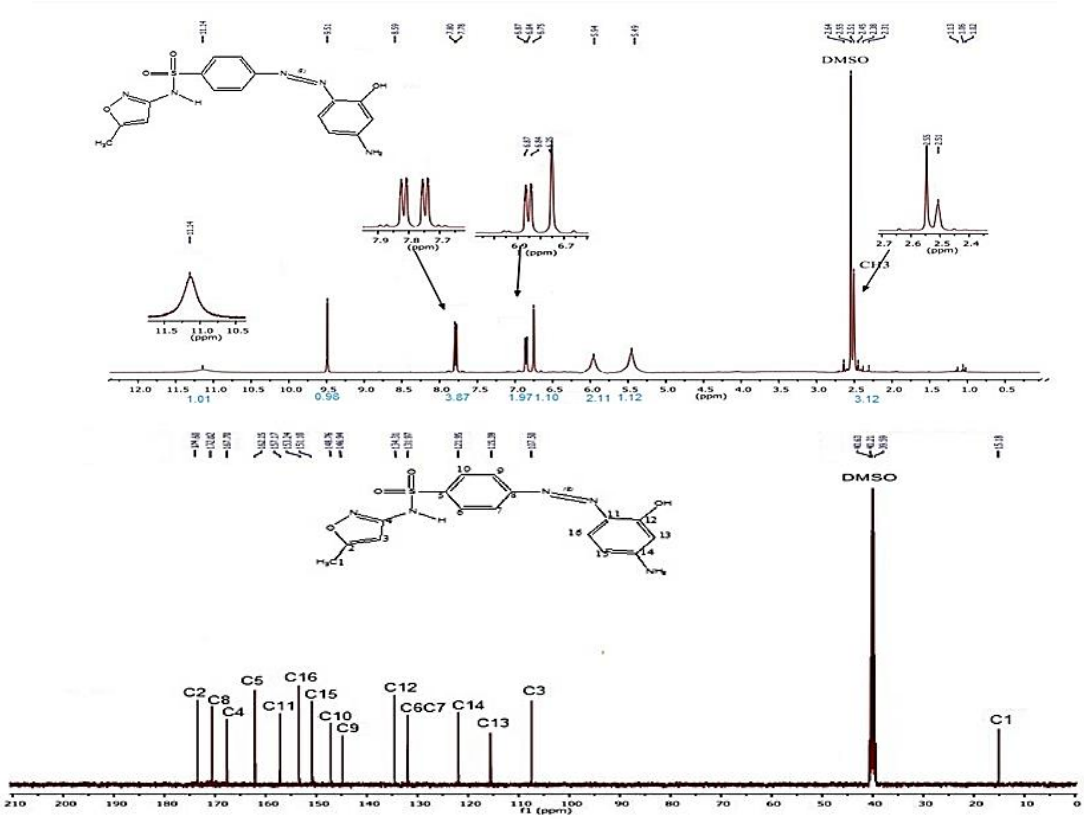

Figure 1:^{1}H &^{13}C-NMR spectra of ligand

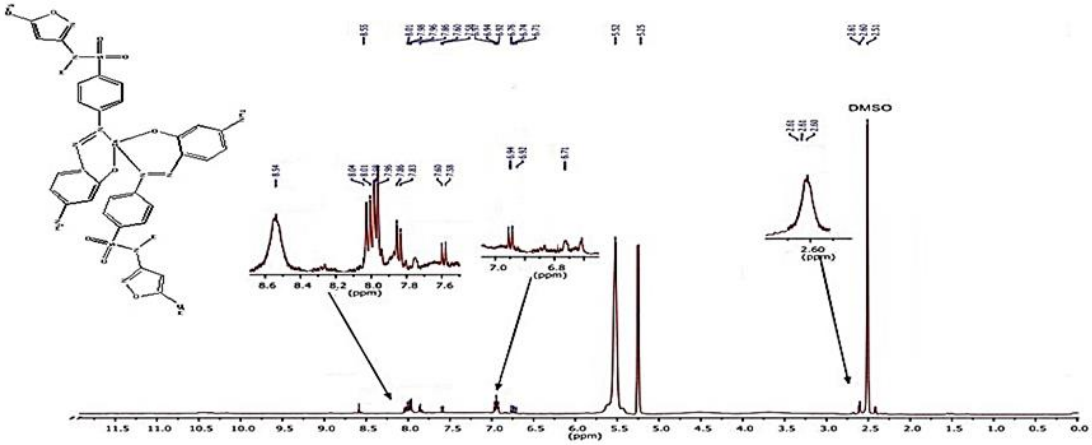

Figure 2: ^{1}HNMR spectra of Zn-complex

Electronic spectra measurements

Table 2 and Figure 3 show the electronic spectrum of ligand (LH). Vanadium complex demonstrates two electronic transitions at 261 and 440 nm in ultra violet region belonging to π→π* and n π→*, respectively, in addition to the two electronic transitions observed at 642 and 687 nm that are attributed to $^2B_{2g}\rightarrow{}^2E_g$ and $^2B_{2g}\rightarrow{}^2B_{1g}$ electronic transitions, whereas the electronic spectrum of copper complex in Figure 4 demonstrates the next electronic transitions, 270 nm, 448 nm and 788nm related to π→π*, n→π* and $^2T_2\rightarrow{}^2E$, respectively, and the zinc electronic spectrum which in turn demonstrates the following electronic transitions: π→π* at 268 nm , n→π* 448 nm and C.T (M→L). In conclusion, along with the electronic spectrum of chromium complex, we also demonstrated the following transitions: In UV-region at 266nm and 442 nm related to π→π* and n→π* transitions, respectively, and C.T transition which proves the occurrence of coordination with ligand in addition to presence of three bands in vis-region at 700 nm, 804 nm and 900 nm belonging to $^4A_{2g}\rightarrow{}^4T_{1g(P)}$, $^4A_{2g}\rightarrow{}^4T_{1g(F)}$ and $^4A_{2g}\rightarrow{}^4T_{2g(F)}$, respectively. The previous electronic data indicate the following geometries: Tetrahedral for both Cr and zinc complexes and square pyramidal, and octahedral geometries for each of VO and Cr complexes, respectively [15-17].

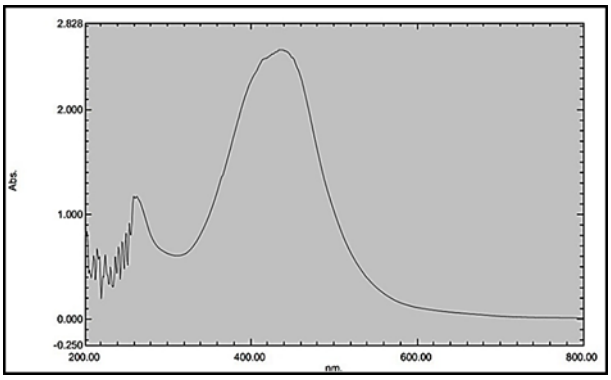

Figure 3: UV-Vis of ligand HL

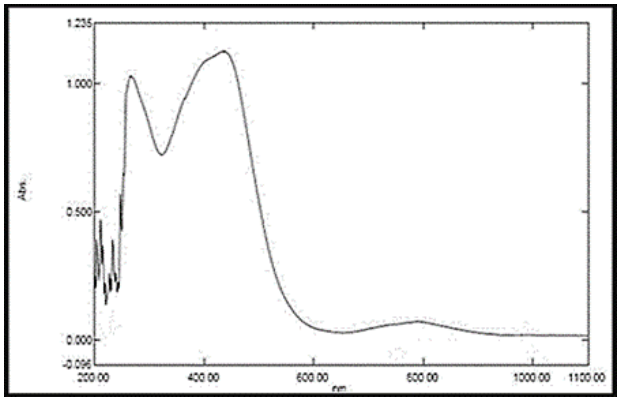

Figure 4: UV-Vis of Cu-complex

Table 2: Electronic spectral data of the metal complexes with LH ligand and molar conductivity in DMSO (1×10^{-3} M)

Compounds	λ nm	ύ cm^{-1}	Abs	ε_{max}	Transition	Geometry	Λm ($S.cm^2.Mol^{-1}$)
Ligand=LH	258	38759.6	1.182	1182	π→π*	--	
	435	22988.5	2.571	2571	n→π *		
$[VO(L)_2]$	261	38314.1	1.183	1183	π→π*	Square Pyramidal	23
	440	22727.2	2.580	2580	n→π *		
	642	15576.3	0.200	200	$^2B_{2g}\rightarrow{}^2E_g$		
	687	14556	0.170	170	$^2B_{2g}\rightarrow{}^2B_{1g}$		
$[Cr(L)_2(H_2O)Cl]$	266	37594	0.551	551	π→π*	Octahedral	21
	442	22624.4	0.612	612	n→π*		
	700	14285.7	0.050	50	$^4A_{2g}\rightarrow{}^4T_{1g(P)}$		
	804	12437.8	0.077	77	$^4A_{2g}\rightarrow{}^4T_{1g(F)}$		
	900	11111.1	0.045	45	$^4A_{2g}\rightarrow{}^4T_{2g(F)}$		
$[Cu\ (L)_2]$	270	37037	1.012	1012	π→π*	Tetrahedral	22
	448	22321.4	1.135	1135	n→π*		
	788	12690.3	0.095	95	$^2T_2\rightarrow{}^2E$		
$[Zn\ (L)_2]$	268	37313.4	1.448	1448	π→π*	Tetrahedral	25
	448	22321.4	1.887	1887	, n→π* C.T (M→L)		

Liquid chromatography–mass spectrometry (LC–MS) measurements

The electron impact of fragmentation was used to acquire mass spectra of the novel ligand and metal complexes. High-resolution MS of the free azo ligand and its complexes, as well as large fragments linked to breakdown products, was obtained in general [18]. Figure 5 shows the electron impact mass spectrum of ligand LH. This ligand molecular weight was calculated to be 373.39g/mol. The spectra showed a peak at 373 m/z, which was attributed to $[M]^+$ and corresponded to a novel azo moiety $C_{16}H_{15}N_5O_4S$. Other distinctive peaks at 239, 141,136 and 97 m/z might be attributed to other pieces. Their brightness indicated the stability of the pieces. Figure-6 depicts the mass spectrum of the VO(II) complex. The complex moiety $C_{32}H_{28}N_{10}O_9C_2V$ had a peak at 811 m/z, which corresponded to the complex moiety $C_{32}H_{28}N_{10}O_9C_2V$ in the spectrum. Other distinctive peaks at 359, 356 and 97 m/z might be attributed to other pieces. Figure 7 depicts the mass spectrum of the Cr(III) complex. The compound moiety $C_{32}H_{30}N_{10}CrO_9S_2Cl$ was identified by a peak at 850 m/z in the spectra. Other distinctive peaks at 477, 237and 136 m/z might be attributed to other pieces. Figure 8 depicts the electron impact mass spectrum of the Cu (II) complex. The complex moiety $C_{32}H_{28}CuN_{10}O_8S_2$ was identified by a peak at 808 m/z in the spectra. Other distinctive peaks at 663, 372, 275 and 161 m/z might be attributed to other pieces. [18-21]. Schemes 3–6 demonstrate the suggest fragmentation routes and structural assignments of pieces.

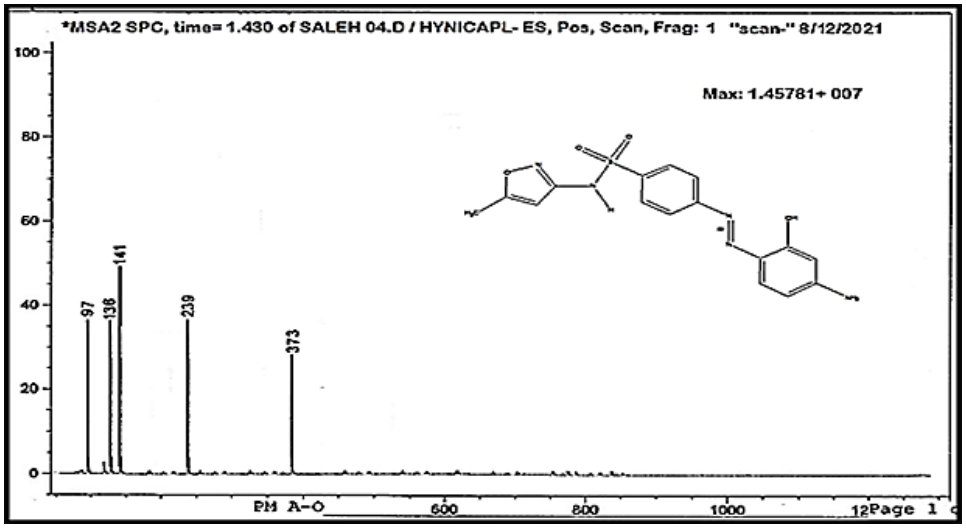

Figure 5: Mass spectrum of ligand (HL)

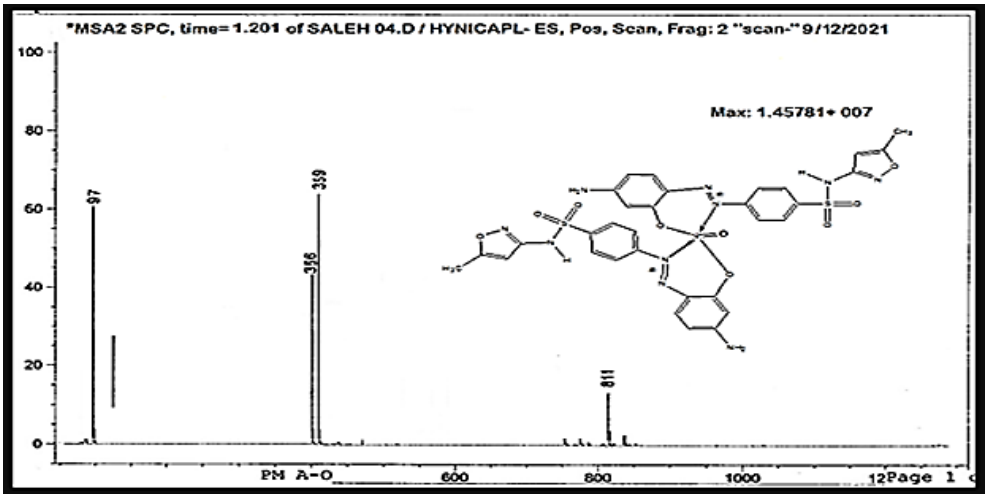

Figure 6: Mass spectrum of vanadium complex

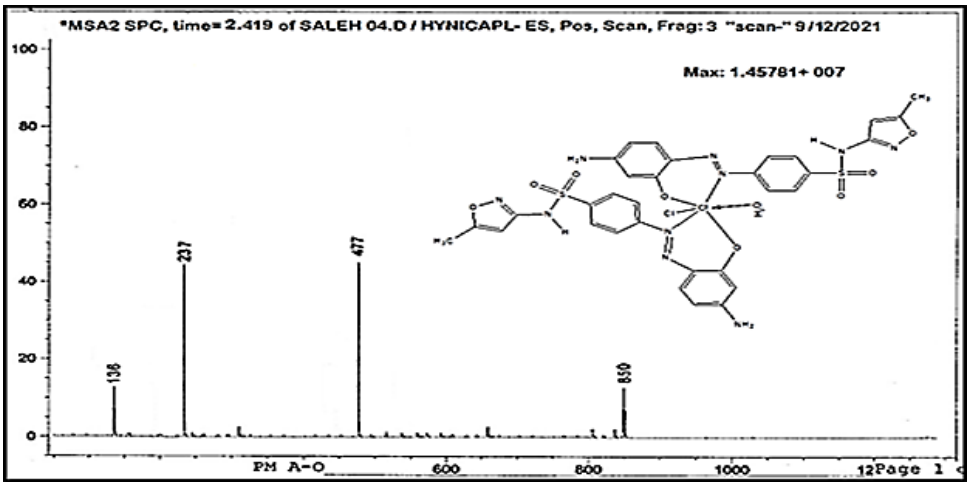

Figure 7: Mass spectrum of chromium complex

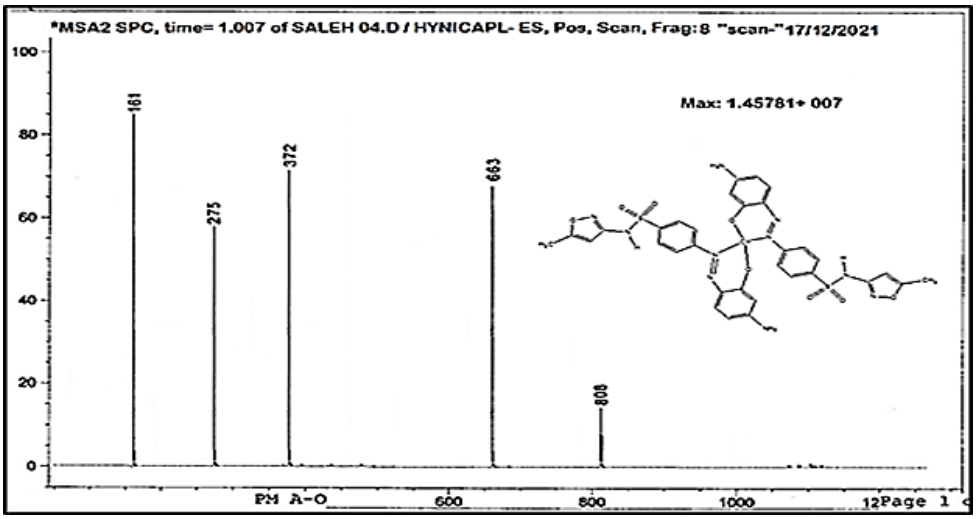

Figure 8: Mass spectrum of copper complex

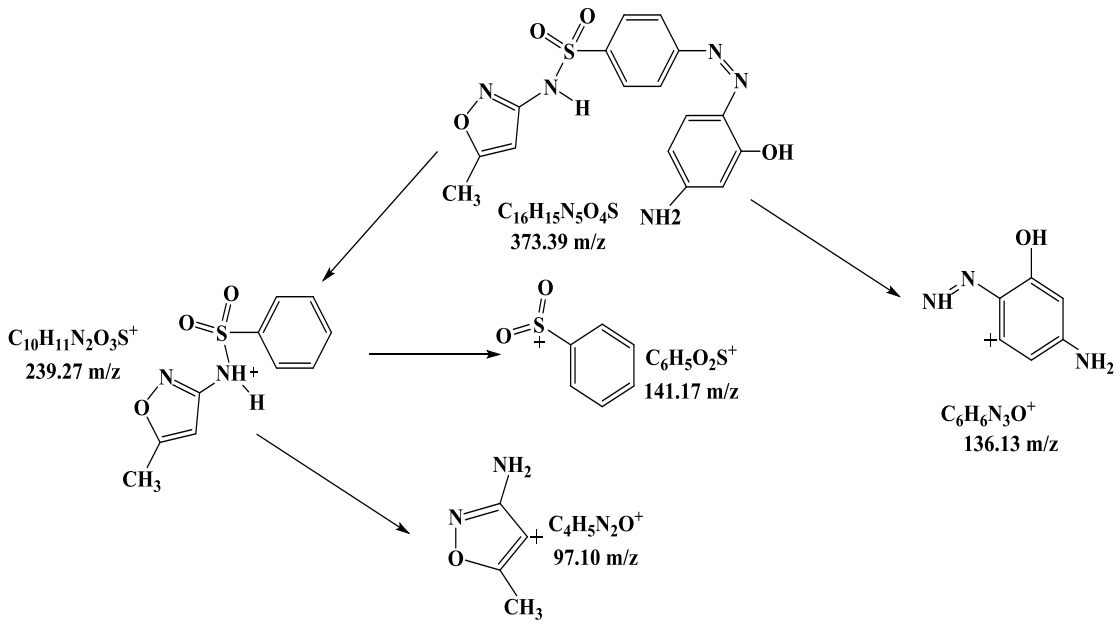

Scheme 3: The fragmentation pattern of ligand (LH)

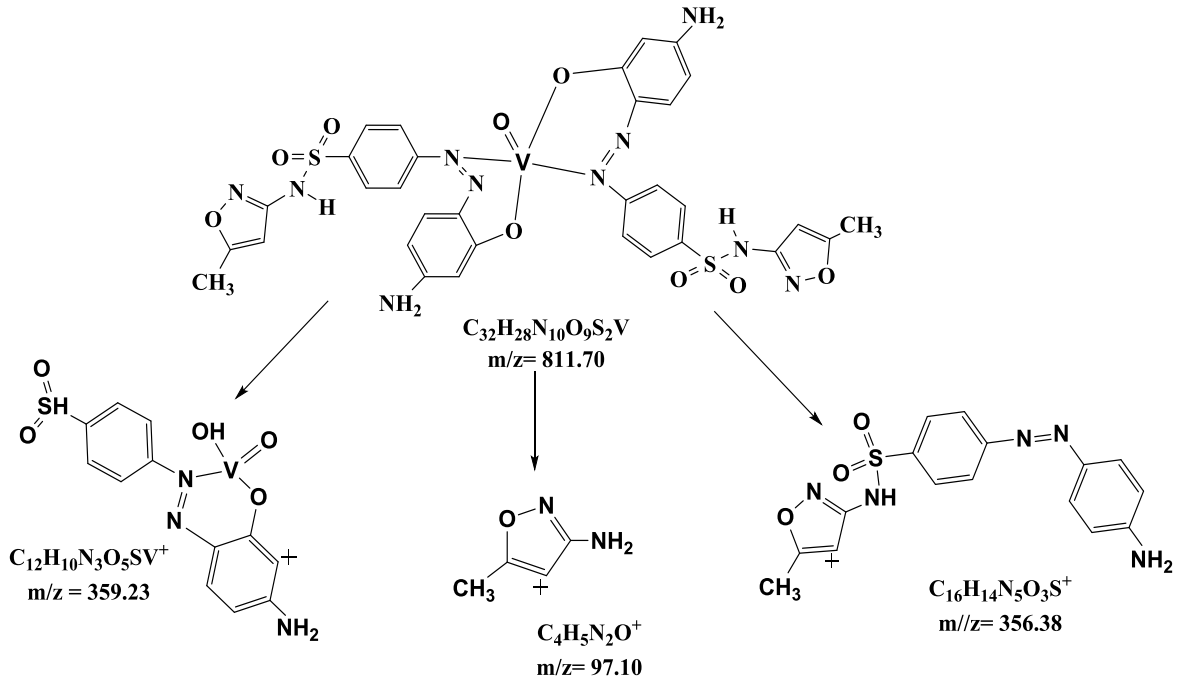

Scheme 4: The fragmentation pattern of VO-complex

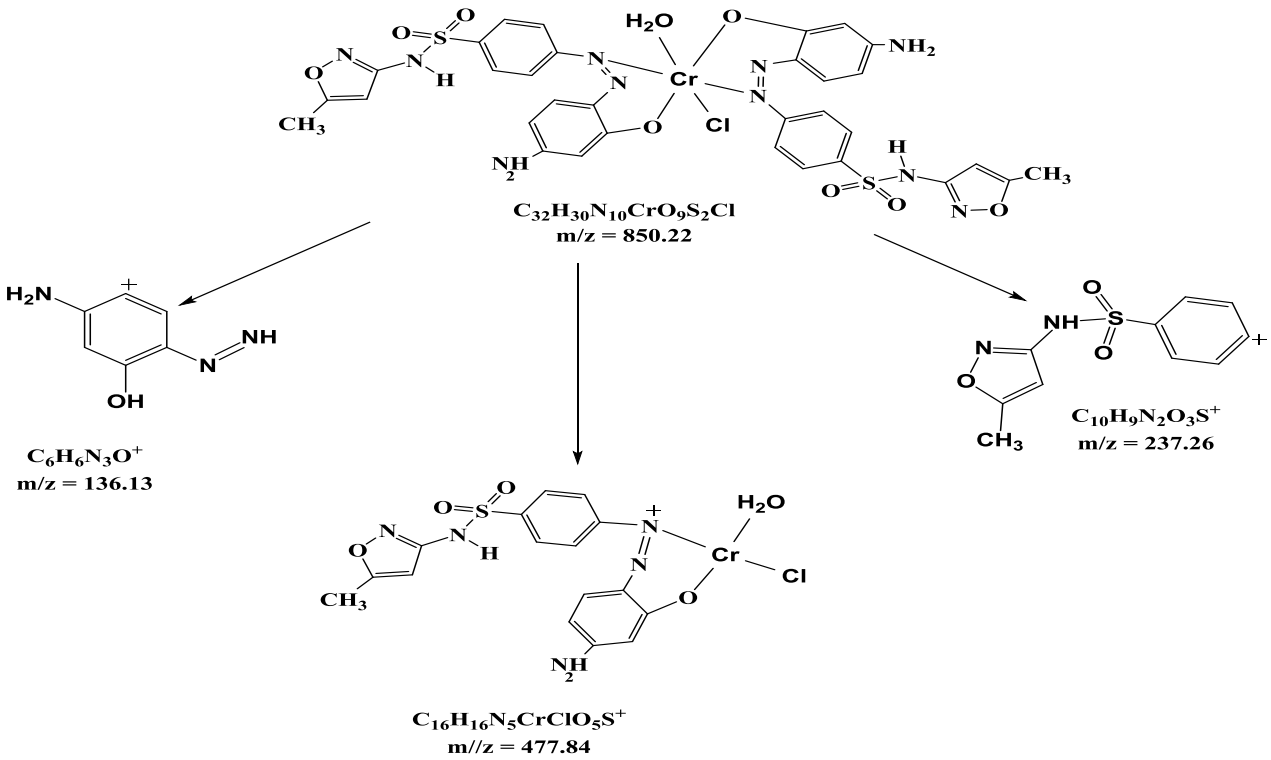

Scheme 5: The fragmentation pattern of Cr-complex

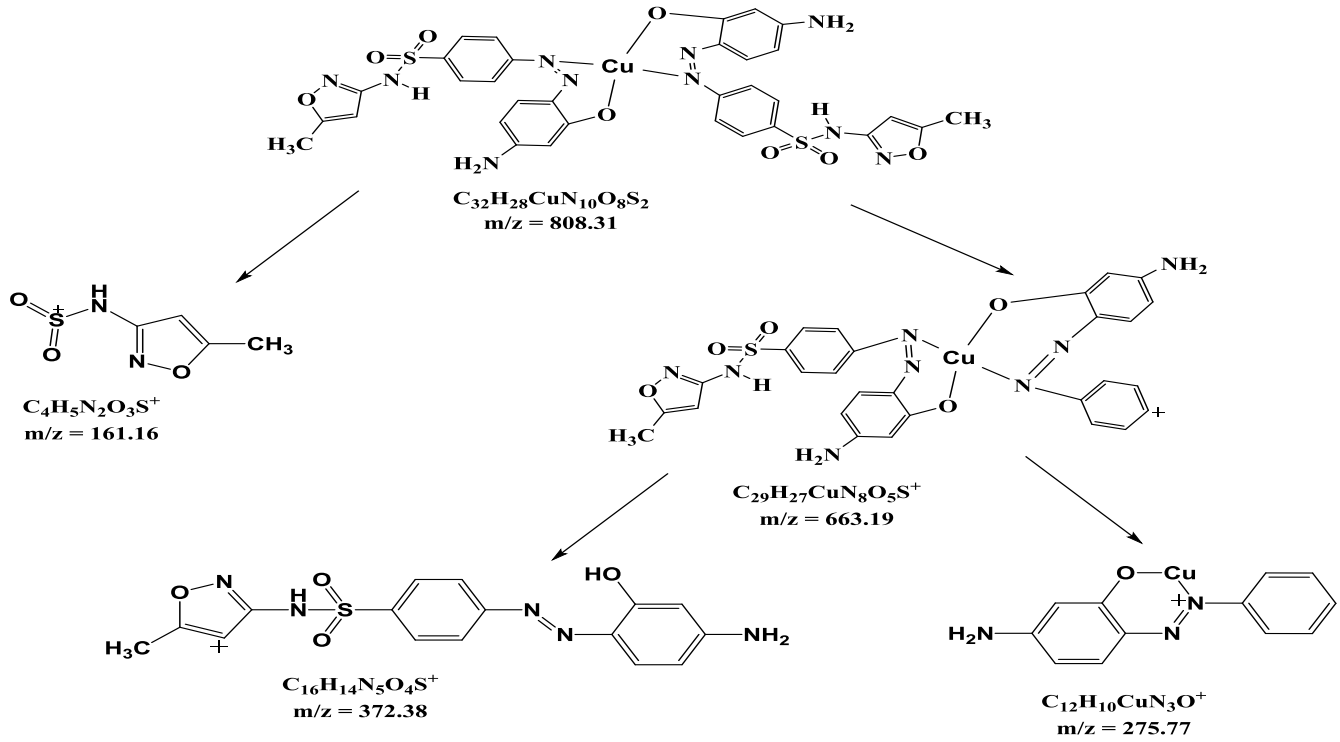

Scheme 6: The fragmentation pattern of Cu-complex

Infrared spectra measurements

FT-IR spectrum of the resulting ligand demonstrates new distinguishable double bands at 1406 and 1467 cm^{-1} attributed to stretching vibrational behavior of azo group N=N, which indicates the ligand formation. On the other hand, the FT-IR spectra of VO(II), Zn(II), Cu(II) and Cr(III) complexes recorded the disappearance of stretching vibrational behavior O-H phenolic group compared with the presence of such vibrational mode in free ligand, proving the occurrence of coordination through phenolic oxygen. Other indications that prove the occurrence of coordination include the observation of new vibrational modes of M-O, M-N and V=O groups at (569-416), (686-447) cm^{-1} and 891 cm^{-1}, respectively, the change in shape, intensity and position of N=N mode compared with the mode of such group in free ligand by 38-58 cm^{-1}. Additionally, the observation of stretching vibrational behavior at 3742, 1579 and 762 belong to the coordinated water molecule with chromium ion [22-28]. All the Fourier transfer returns are listed in Table 3 below.

Table 3: FT-IR returns of ligand and its complexes

Compound	ν(NH_2)	ν(NH)	ν(C-H) aromatic	(C-H)ν aliphatic	N=N	SO_2	(M-O)	M-N	(H_2O)	Other bands
Ligand	3377 3318 1618	3142	3042	2927	1467 1406	1035 1091	--	--		(OH) phenolic 3492
$[VO(L)_2]$	3323 3284 1624	3189	3009	2927	1461 1436	1045 1086	416	536		(V=O) 891
$[Cr(L)_2(H_2O)Cl]$	3458 3379 1625	3285	3079	2923	1451 1410	1039 1110	525	595	3742 1579 762	-
$[Cu(L)_2]$	-	3197	3027	2927 2849	1409 1435	1042 1089	416	537	-	-
$[Zn(L)_2]$	-	3200	3055	2954 2888	1400 1433	1044 1088	411	509	-	-

Study of thermo gravimetric analysis for the compounds by TGA and DSC Curve

The results of thermogravimetric analyses and DSC of azo and its complexes are given in Tables 4 and 5 and Figures 9–16. The thermograms were performed in the range of 30–700C at a heating rate of 10 °C/min in nitrogen atmosphere. They displayed an agreement in weight loss between their consequences achieved from the thermal decomposition and the considered values, supporting the results of elemental analysis and confirming the proposed formulae [29–33] as shown in Scheme 7. The prepared compounds showed a decomposition of the compounds in the thermo gravimetric decomposition curve, where the ligand showed little thermal stability at 41 °C, similar to the little stability complexes in the range of 150 °C for Cr complex, indicating the presence of water molecules in the Cr complex, either water hydrate or Aqua. Finally, the pyrolysis steps of the ligand LH and its complexes were determined and predicted the steps that involved the amount of the released and absorbed energy in DSC curve.

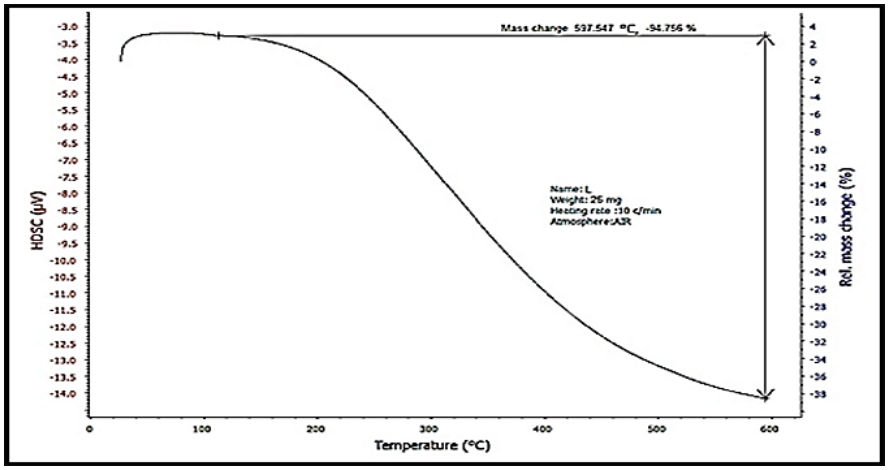

Figure 9: TGA curve of the ligand (HL)

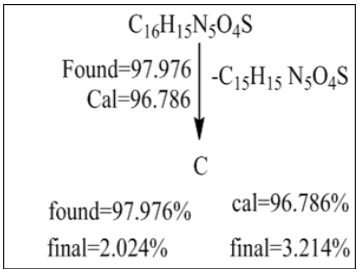

Scheme 7: Steps of pyrolysis of ligand (HL)

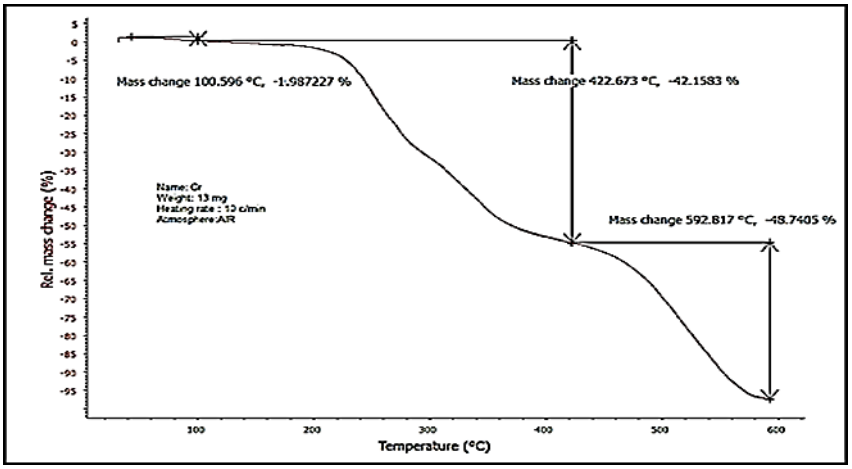

Figure 10: TGA curve of Cr-complex

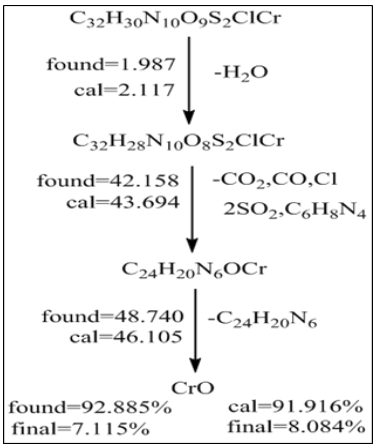

Scheme 8: Steps of pyrolysis of Cr-complex

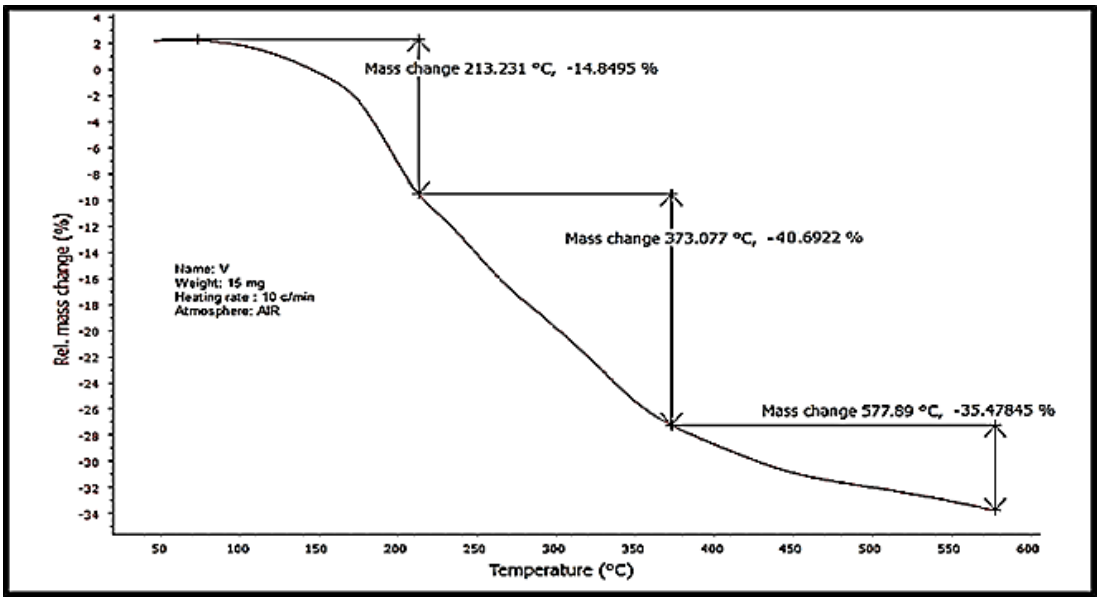

Figure 11: TGA curve of VO^{2+} complex

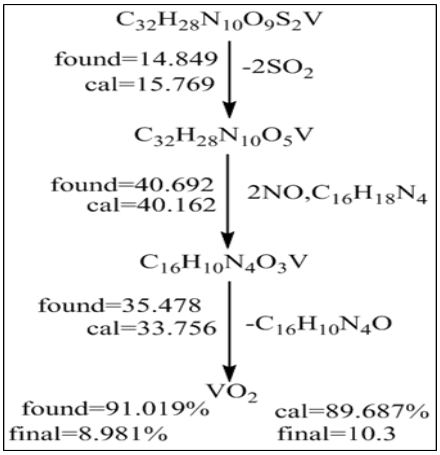

Scheme 9: Steps of pyrolysis of VO2+complex

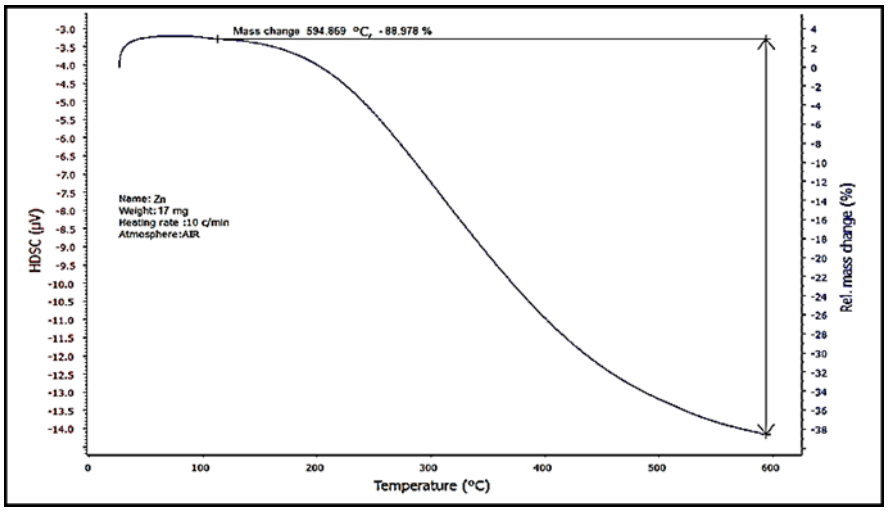

Figure 12: TGA curve of Zn2+ complex

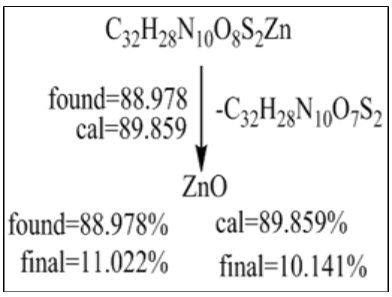

Scheme 10: Steps of pyrolysis of Zn2+ complex

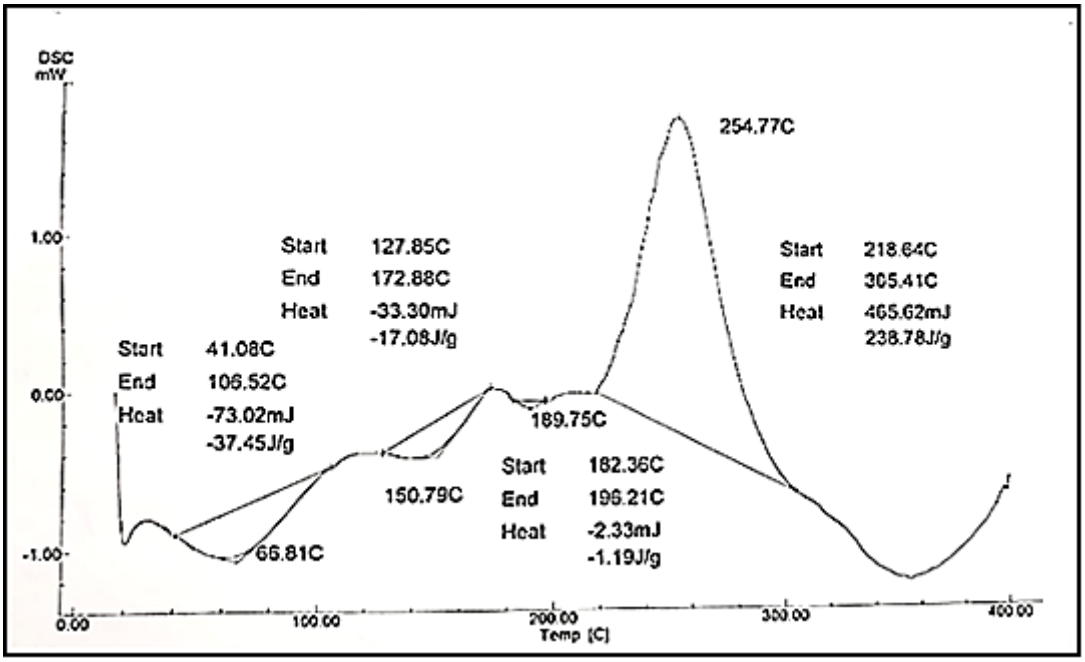

Figure 13: DSC curve of ligand (HL)

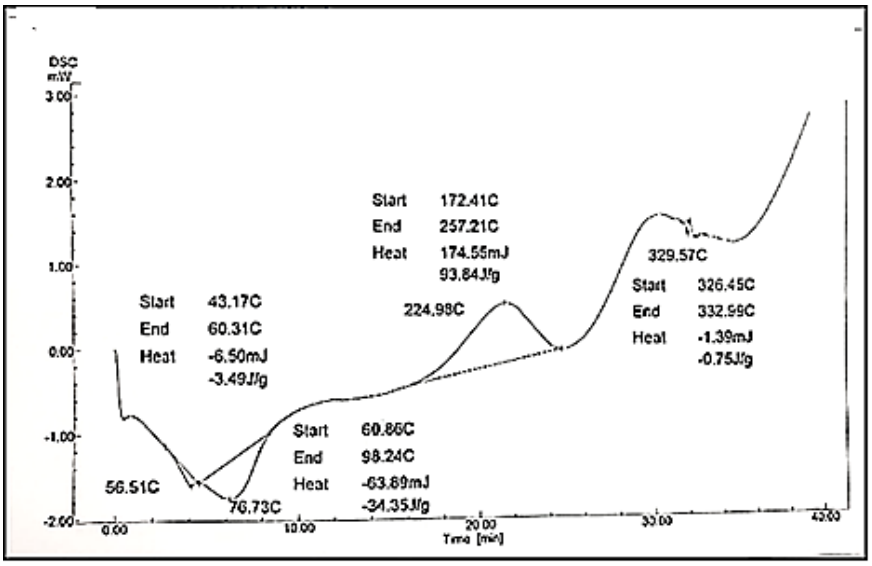

Figure 14: DSC curve of VO-complex

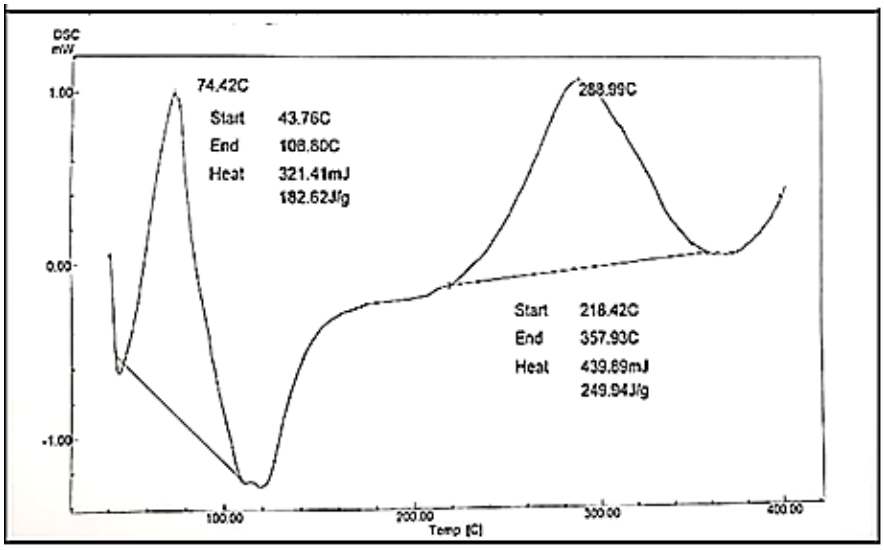

Figure 15: DSC curve of Cr-complex

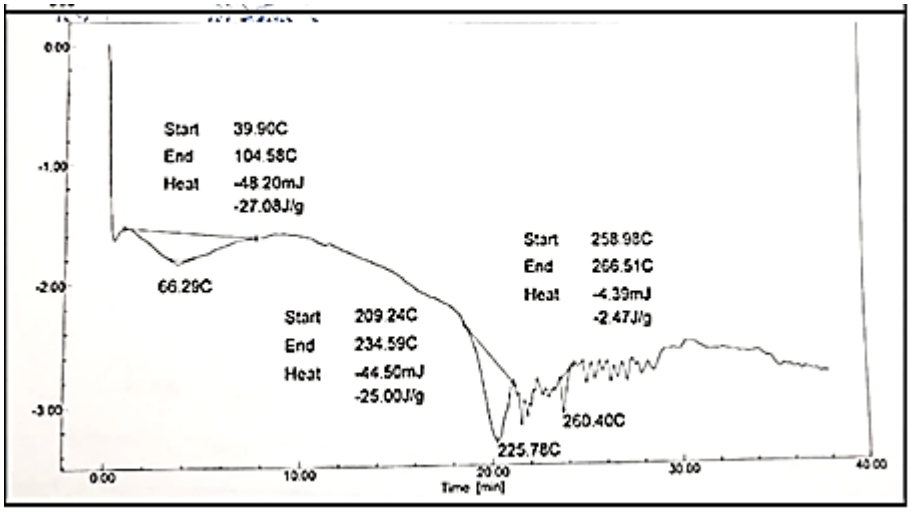

Figure 16: DSC curve of Zn-complex

Table 4: DSC data of the ligand and its complexes

Compound	°C/T_i	T_f/°C	Maximum temperature point ˚C	Type	ΔH J/g
Ligand HL	41.08	106.52	66.81	endothermic	-37.45
	127.85	172.88	150.79	endothermic	-17.08
	182.36	196.21	189.75	endothermic	-1.19
	218.64	305.41	254.77	exothermic	238.78
$[VO(L)_2]$	43.17	60.31	56.51	endothermic	-3.49
	60.86	98.24	76.73	endothermic	-34.35
	172.41	257.21	224.98	exothermic	93.84
	326.45	332.99	329.57	endothermic	-0.75
$[Cr(L)_2(H_2O)Cl]$	43.76	108.80	74.42	exothermic	182.6
	218.42	357.93	288.929	exothermic	244.94
$[Zn(L)_2]$	39.90	104.58	66.29	endothermic	-27.08
	209.24	234.59	225.78	endothermic	-25.00
	258.98	266.51	260.40	endothermic	-2.47

Table 5: TGA records for the ligand and its related complexes

Compound	T_i / °C	T_f/ °C	T_{DTG} max	% Estimated (calculated)		(Remnant) Remnant	Assignment
				Mass loss	Total mass loss		
(HL)	119.634	597.547	306.763	97.976 (96.786) 2.024 (3.214)	97.976 (96.786)		$-C_{15}H_{15}N_5O_4S$ C
$[VO(L)_2]$	79.136 213.231 373.077	213.231 373.077 577.89	166.397 279.264 471.357	4.89 (15.769) 40.692(40.162) 35.478(33.756)	91.06 (89.687)	8.94 (10.313)	$-2SO_2$ $-2NO,C_{16}H_{18}N_4$ $-C_{16}H_{10}N_4O$ VO_2
$[Cr(L)_2(H_2O)Cl]$	43.344 100.596 422.673	100.596 422.673 592.817	80.864 377.796 517.782	1.987 (2.117) 42.158 (43.158) 48.740 (46.105)	92.885 (91.38)	7.115 (8.62)	$-H_2O$ $CO_2,CO,Cl,2SO_2$ $C_6H_8N_4$ $-C_{24}H_{20}N_6$ CrO
$[Zn(L)_2]$	119.36	594.869	348.85	88.978 (89.859)	88.978 (89.859)	11.022 (10.141)	$-C_{32}H_{28}N_{10}O_7S_2$ ZnO

Vital diagnosis

The vita vigor of azo entities and their related-compounds including *S aureus, P aeruginosa* Bacteria and Fungi *P expansum, F graminearum, M phasealina*, and *C albicans* bacteria was examined. The incoming returns were recorded in schedule-6 below and compared with DMSO. Azo entity demonstrates observational-inhibitions, either at high concentrations-A or at low concentrations-B. There were variations recorded at each of the concentrations employed [34-36].

Table 6: Vital returns

Compounds	Positive and negative bacteria				Fungi							
type	*S.T*		*P.A*		*Pe.*		*F.M*		*M.P*		*Ca.a*	
Conc.	A	B	A	B	A	B	A	B	A	B	A	B
$CrCl_3.6H_2O$	15	12	16	15	38	28	38	33	——	——	——	—
LH	12	——	12	——	——	——	——	—	——	——	——	—
$[Cr(L)_2(H_2O)Cl]$	16	——	15	——	20	18	28	22	24	16	——	—
$ZnCl_2$	40	25	23	18	30	18	26	15	0	0	20	10
$[Zn(L)_2]$	20	0	15	0	13	0	0	0	25	16	0	0
Control	0	0	0	0	0	0	0	0	0	0	0	0

S.T =Staphylococcus aureus, P.A.= Pseudomonas aeruginosa, Pe.=Penicilliumexpansum, M.P= Macrophominaphaseolina and Candida albicans =Ca.a, A= conc. B= dilute.

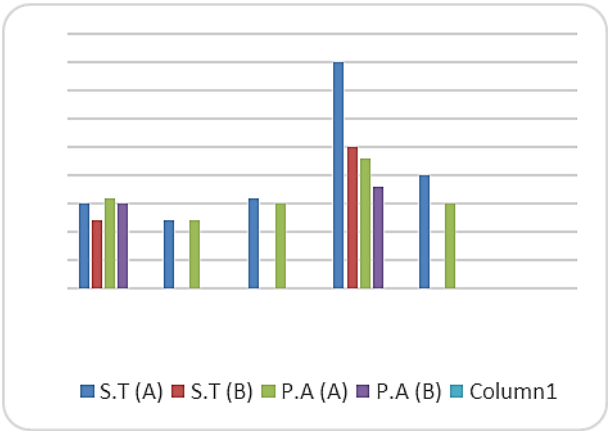

Figure 17: Microbiological investigations on Bacteria

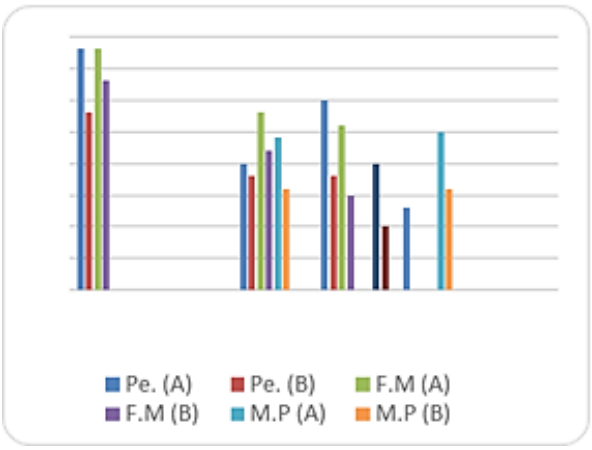

Figure 18: Microbiological investigations on Fungi

Study of complexes in gas stat (theoretical studies)

Electrostatic potentials

Theoretical study for the formed entity (LH) was accomplished at its gaseous state in order to detect the stretching vibrations and Fourier transform spectra and make a competition for them with the practical returns, as well as to detect the mistake percentage, and so forth for the complexes [37].

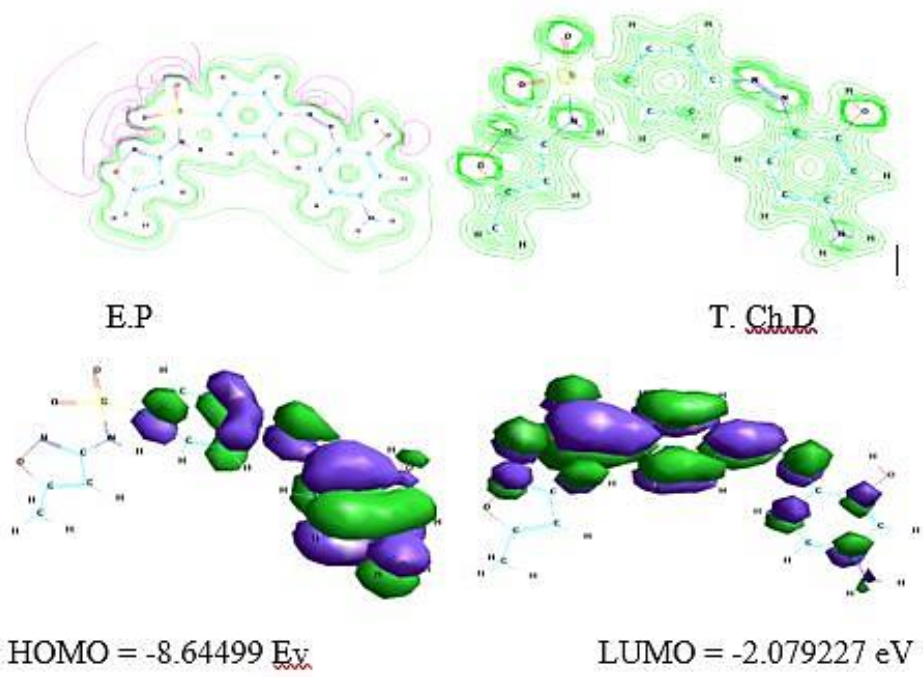

Figure 19: Electrostatic potential (HOMO and LUMO) as 2D and 3D contours for LH

Optimal energies

Hyper Chem 8 was employed in mech. calculations resembling theoretical (ΔHf°) and (ΔEb) for each synthesized entity as represented in Table in 7.

Table 7: Conformation energetic (in KJ.mol-1) for Naringin and its metal complexes

Compound	ΔH°_{f} Heat of formation	ΔE_b Binding energy	Total energy	Dipole moment
HL	172.11487	-4.213.2911	-98871.01680	10.561
V-complex	-21.21375	-8.8527412	-7878.79461	48.970
Cr-complex	-14.84315	-10.979864	-9519.75314	9.847

Optimized vibrational spectra for ligand

The vibrational spectra of the free ligand and their metal complexes were calculated (Table 8). The theoretically calculated wavenumbers for this ligand showed that some deviations from the experimental values were generally acceptable in theoretical calculations [26]. The most diagnostic calculated vibrational frequencies were chosen for the assignment of ligand (HL) and metal complexes, and their respective experimental vibrational modes as shown in Table 8. The results obtained for the theoretical calculations of the frequencies agreed well with those of the experimental values.

Optimized geometries of LH and their complexes

All theoretically probable structures of free ligand and their complexes were calculated by PM3 method in gas phase to search for the most probable model aiming at building the stable structure.

Table 8: Comparison between the experimental and theoretical vibrational frequencies (cm^{-1}) for free ligand metal complexes

Ligand HL	ν (OH)	ν (NH_2)	ν (NH)	(C-H) aliphatic	(C-H) Aromatic	ν (SO_2)	ν (N=N)
Found	3492	3377 3318 1618	3142	2927	3042	1035 1091	1467 1406
Calc.	3500	3401 3280 1706	3200	3010	3117	1121 997	1490 1469
mistake %	0.002	0.007 -0.011 0.051	0.018	0.027	0.024	0.076 -0.094	0.015 0.042

Conclusion

In this research we prepared new azo ligand 4-amino- *N*- (5- methyl- isaxazol- 3- yl)-benzenesulfonamide, by reacting the diazonium salt of sulfamethoxazole with coupling compound 3-amino phenol. Spectroscopic techniques (UV-Vis, FTIR, ^{1}H and ^{13}C-NMR, and LC-Mass) as well as micro elemental analyses (C.H.N.O) and TGA and SDC were used to identify the azo ligand. Complexes of (Zn(II), Cr(III), Cu(II) and VO(II)) were produced and characterized by atomic absorption, elemental microanalysis, infrared, LC-Mass, TGA, DSC and UV-Vis spectral techniques, as well as conductivity and magnetic quantifications. The resultant complexes were gave the following geometries; tetrahedral for each of Cu and Zn complexes, square pyramidal for VO complex and octahedral for Cr complex. The ligand and some of its complexes and their corresponding metal salts were biologically investigated toward bacteria and fungi in various concentrations and noticed that, their activity decreases at lower concentrations.

Acknowledgments

Department of Chemistry, College of Science for Women, University of Baghdad and Prof. Dr. Abbas Ali Salih Al-Hamdani.

Funding

This research did not receive any specific grant from fundig agencies in the public, commercial, or not-for-profit sectors.

Authors' contributions

All authors contributed toward data analysis, drafting and revising the paper and agreed to responsible for all the aspects of this work.

Conflict of Interest

We have no conflicts of interest to disclose.

ORCID:

Shaima Mohammed Reda

https://www.orcid.org/0000-0002-9700-7211

Abbas Al-Hamdani

https://orcid.org/0000-0002-2506-986X

References

[1]. Shankarling G.S., Deshmukh P.P., Joglekar A.R., *J. Environ. Chem. Eng*., 2017, **5**:3302 [Crossref], [Google Scholar], [Publisher]

[2]. Gürses A., Açıkyıldız M., Güneş K., Gürses M.S., *Dyes Pigm.*, 2016, 31–45 [Crossref], [Google Scholar], [Publisher]

[3]. Shah M., *Int. J. Environ. Bioremediat. Biodegrad*., 2014, **2**:231 [Google Scholar], [Publisher]

[4]. Al-Hamdani A.A.S., Ahmed S.D., Shake S.H., Hassan Z.A., *Baghdad Sci. J.*, 2016, **13** [Google Scholar]

[5]. Al-Hamdani A.A.S., Shaalan N., Hassan S.S., Hasan Z.A., *Baghdad Sci. J.*, 2016, **13** [Google Scholar]

[6]. Al-Hamdani A.A.S., Balkhi A., Falah A., Shaker S.A., *J. Chi. Chem. Soc.*, 2015, **60**:2774 [Crossref], [Google Scholar], [Publisher]

[7]. Al Zoubi W., Al-Hamdani A.A.S., Putu Widiantara I., Hamoodah R.G., Ko Y.G., *J. Phys. Org. Chem.*, 2017, **30**:e3707 [Crossref], [Google Scholar], [Publisher]

[8]. Al-Hamdani A.A.S., Hamoodah R.G., *Baghdad Sci. J.*, 2016, **13**:770 [Google Scholar], [Publisher]

[9]. Benkhaya S., Achiou B., Ouammou M., Bennazha J., Younssi S.A., M'rabet S., El Harfi A., *Mater. Today Commun.*, 2019, **19**:212 [Crossref], [Google Scholar], [Publisher]

[10]. Al Zoubia W., Al-Hamdani A.A.S., Mosab K., *Appl. Organomet. Chem.*, 2016, **30**:810 [Crossref], [Google Scholar], [Publisher]

[11]. Al-Hamdani A.A.S., Abdel M.B., Falah A., Shayma A.S., *J. Saudi Chem. Soc.*, 2016, **20**:487 [Crossref], [Google Scholar], [Publisher]

[12]. Saeed A.M., AlNeyadi S.S., Abdou I.M., *Heterocycl. Comm.*, **2020**, **26**:192 [Crossref], [Google Scholar], [Publisher]

[13]. Al Zoubi W., Al-Hamdani A.A.S., Ko Y.G., *Sep. Sci. Technol.*, 2017, **52**:1052 [Crossref], [Google Scholar], [Publisher]

[14]. Kuate M., Conde M.A., Nchimi K.N., Paboudam A.G., Ntum S.J.E., Ndifon P.T., *Int. J. Org. Chem.*, 2018, **8**:298 [Crossref], [Google Scholar], [Publisher]

[15]. Al Zoubi W., Al-Hamdani A.A., Ahmed S.D., Ko Y.G., *Appl. Organomet. Chem*., 2018, **32**:e3895 [Crossref], [Google Scholar], [Publisher]

[16]. Obaid S.M.H., Jarad A.J., Al-Hamdani A.A., *J. Phys.: Conf. Ser.*, 2020, **1660**:012028 [Publisher]

[17]. Suleman V.T., Al-Hamdani A.A.S., Ahmed S.D., Jirjees V.Y., Khan M.E., Dib A., Al Zoubi W., Ko Y.G., *Appl. Organomet. Chem.*, 2020, **34**:e5546 [Crossref], [Google Scholar], [Publisher]

[18]. Al-Hamdani A.A.S., Al Zoubi W., *Spectrochim. Acta A Mol. Biomol. Spectrosc.,* 2015, **137**:75 [Crossref], [Google Scholar], [Publisher]

[19]. Al Zoubi W., Al-Hamdani A.A.S., Susan D.A., Hassan M.B., Al-Luhaibi R.S.A., Adnan D., Young G.K., *J. Phys. Org Chem.,* 2018, **32**:e3916 [Crossref], [Google Scholar], [Publisher]

[20]. Ye Z., De Boni L., Neves U.M., Mendonça C.R., Bu X.R., *Tetrahedron Lett.*, 2009, **50**:1371 [Crossref], [Google Scholar], [Publisher]

[21]. Kareem M.J., Al-Hamdani A.A.S., Ko Y.G., Al Zoubi W., Mohammed S.G., *J. Mol. Struct.*, 2021, **1231**:129669 [Crossref], [Google Scholar], [Publisher]

[22]. Obaid S.M.H., Sultan J.S., Al-Hamdani A.A.S., *Indones. J. Chem.*, 2020, **20**:1311 [Crossref], [Google Scholar], [Publisher]

[23]. Al-Hamdani A.A.S., Al-Khafaji N.R., Shaalan N., *Res. J. Pharm. Biol. Chem. Sci.*, 2017, **8**:740 [Crossref], [Google Scholar], [Publisher]

[24]. Al-Hamdani A.A.S., Al-dulyme N.K.G., Ibn *AL-Haitham J. Pure Appl. Sci.*, 2017, **30**:69 [Google Scholar], [Publisher]

[25]. Al Zoubi W., Mohamed S.G., Al-Hamdani A.A.S., Mahendradhany A.P., Ko Y.G., *RSC Adv.*,

2018, **8**:23294 [Crossref], [Google Scholar], [Publisher]
[26]. Al-Hamdani A.A.S., Hasan Z.A.A., *Baghdad Sci. J.*, 2016, **13**:511 [Google Scholar], [Publisher]
[27]. Jirjees V.Y., Suleman V.T., Al-Hamdani A.A.S., Ahmed S.D., *Asian J. Chem.*, 2019, **31**:2430 [Crossref], [Google Scholar], [Publisher]
[28]. Al Zoubi W., Al-Hamdani A.A.S., Sunghun B., Ko Y.G., *Rev. Inorg. Chem.,* 2021, **41**:213 [Crossref], [Google Scholar], [Publisher]
[29]. Al Zoubi W., Kim M.J., Al-Hamdani A.A.S., Kim Y.G., Ko Y.G., *Appl. Organomet. Chem.*, 2019, **33**:e5210 [Crossref], [Google Scholar], [Publisher]
[30]. Jirjees V.Y., Al-Hamdani A.A.S., Wannas N.M., Faeqad A.R., Dib A., Al Zoubi W., *J. Phys. Org. Chem.*, 2021, **34**:e4169 [Crossref], [Google Scholar], [Publisher]
[31]. Bal S., Bal S.S., *Adv. Chem*., 2014; **2014**:1 [Crossref], [Google Scholar], [Publisher]
[32]. Samy M.E., Moamen S.R., Fawziah A.A., Reham Z.H., *Int. J. Environ. Res. Public Health*., 2021, **18**:8030 [Crossref], [Google Scholar], [Publisher]
[33]. Kirill V.Y., Aleksandr S.S., Werner K., Sergey A.G., *Molecules*, 2020, **25**:768 [Crossref], [Google Scholar], [Publisher]
[34]. Kareem M.J., Al-Hamdani A.A.S., Jirjees V.Y., Khan M.E., Allaf A.W., Al Zoubi W., *J. Phys. Org. Chem.*, 2020, **34**:e4156 [Crossref], [Google Scholar], [Publisher]
[35]. Jirjees V.Y., Al-Hamdani A.A., Wannas N.M., A. R F, Dib A., Al Zoubi W., *J. Phys. Org. Chem.*, 2021, **34**:e4169 [Crossref], [Google Scholar], [Publisher]
[36]. Jirjees V.Y., Suleman V.T., Al-Hamdani A.A., Ahmed S.D., *Asian J. Chem.,* 2019, **31**:2430 [Google Scholar]

HOW TO CITE THIS ARTICLE
Shaima Mohammed Reda, Abbas Ali Salih Al-Hamdani. Synthesis, Characterization, Thermal Analysis and Bioactivity of Some Transition Metals Complexes with New Azo Ligand. *Chem. Methodol.*, 2022, 6(6) 475-493
https://doi.org/10.22034/CHEMM.2022.335815.1468
URL: http://www.chemmethod.com/article_148572.html